Analyst

Accepted Manuscript

ROYAL SOCIETY OF CHEMISTRY

www.rsc.org/analyst

Cite this: DOI: 10.1039/c0xx00000x

www.rsc.org/xxxxxx

ARTICLE TYPE

Trap and Track: Designing Self-reporting Porous Si Photonic Crystals for Rapid Bacteria Detection†

Naama Massad-Ivanir,[a] Yossi Mirsky,[b] Amit Nahor,[b] Eitan Edrei,[b] Lisa M. Bonanno-Young,[a] Nadav Ben Dov,[a] Amir Sa'ar[b] and Ester Segal*[a,c]

Received (in XXX, XXX) Xth XXXXXXXXX 20XX, Accepted Xth XXXXXXXXX 20XX

DOI: 10.1039/b000000x

The task of rapid detection and identification of bacteria remains a major challenge in both medicine and industry. This work introduces a new concept for the design of self-reporting optical structures that can detect and quantify bacteria in real-time. The sensor is based on a two-dimensional periodic structure of porous Si photonic crystals in which the pore size is adjusted to fit the target bacteria cells (*Escherichia coli*). Spontaneous bacteria capture within the pores induces measurable changes in the zero-order reflectivity spectrum collected from the periodic structure. Confocal laser microscopy and electron microscopy confirm that the *Escherichia coli* cells are individually imprisoned within the porous array. A simple model is suggested to correlate the optical readout and the bacteria concentration and its predictions are found to be in good agreement with experimental results. In addition, we demonstrate that sensing scheme can be easily modified to potentially allow monitoring of concentration, growth and physiological state of bacteria cells. This generic platform can be tailored to target different microorganisms by tuning the array periodicity and its surface chemistry for rapid and label-free detection outside the laboratory environment.

1. Introduction

Porous Si (PSi) and oxidized PSi ($PSiO_2$) matrices are promising platforms for biological sensing.[1-10] Biosensing of various chemical and biological analytes, such as fluorescent molecules,[11] drug molecules,[12] DNA,[13, 14] and proteins[4, 5, 7, 9, 15] was successfully demonstrated. Many of these studies employ the rather simple and yet efficient method of reflective interferometric Fourier transform spectroscopy (RIFTS) to monitor biological interaction within mesoporous Si thin films.[4, 5, 16, 17] However, these detection schemes are not applicable for targeting large biological species (from few hundreds of nanometers up to several microns and more) such as viruses, bacteria and bacterial spores, as these species are too large to penetrate into the pores.

Alternative PSi-based biosensing approaches monitor changes in the intensity of the reflectivity spectrum upon direct capture of larger cellular targets e.g., bacteria cells, on the top surface of the PSi nanostructure.[8, 18-22] While, these sensing platforms may provide relatively high sensitivity (dynamic range of 10^3-10^6 cell mL^{-1} and detection limit as low as 10^2 cell mL^{-1}) and rapid response toward the target cells, they do not take advantage of the large porous volume and maybe prone to intensity fluctuations under certain conditions.

Here, we report on the design of a self-reporting PSi optical structure for rapid detection and monitoring of bacteria cells. Our approach extends the current sensing capabilities of PSi to also include micron-scale targets. *Escherichia coli* (*E. coli*) is chosen as highly relevant model gram-negative bacteria. In recent years there is an immense effort to develop new bioassays and biosensors for the rapid detection of bacteria in general and pathogenic bacteria in particular.[23-28] Other important challenges are the ability to distinguish between live and dead bacteria[29] and to monitor bacterial growth, which is acute for many clinical applications e.g., faster antimicrobial susceptibility testing.[30, 31] Despite the significant progress in the field, current technologies lack the ability to detect and monitor microorganisms in "real time" or outside the laboratory environment.[22, 23, 32] Therefore, this study is designed as a response to these important challenges.

2. Experimental section

2.1 Materials

P-type Si wafers (10-30 Ω-cm resistivity, ‹100› oriented, B-doped) are purchased from Siltronix Corp. Aqueous HF (49%), N,N-dimethylformamide (DMF), hydrogen peroxide 30% (H_2O_2), Amonium hydroxide solution 25% (NH_3), toluene, acetonitrile and absolute ethanol were supplied by Merck. Bis(N-succinimidyl)carbonate (SC), (3-aminopropyl)triethoxysilane (APTES), glutaraldehyde solution and D-mannosamine hydrochloride are obtained from Sigma Aldrich Chemicals. All reagents are of analytical grade and used as received. Phosphate buffered saline (PBS) at pH 7.4 was prepared by dissolving 50 mM Na_2HPO_4, 17 mM NaH_2PO_4, and 68 mM NaCl in purified water (18.2 MΩ). *E. coli* bacteria expressing green fluorescent protein (pGFP) were generously supplied by Prof. Sima Yaron (Technion).

2.2 Preparation of macro-PSi array structures (MPSiAS)

Two-dimensional (2D) ordered arrays of macro-PSi structure, with hexagonal or orthogonal lattice patterns and a periodicity in

Cite this: DOI: 10.1039/c0xx00000x

www.rsc.org/xxxxxx

ARTICLE TYPE

the range of 2-4 μm, are prepared from p-type <100> Si wafer (with a typical resistivity of 10-30 Ω-cm). First, a 2D pattern of inverted pyramid grooves is defined on top of the wafer by alkaline etching via a photolithographic oxide mask. Then, anodization is carried out under dark conditions, using an electrolyte solution of HF (49%) and DMF (1:7 v/v), at a constant current density (30 mA cm^{-2}, 125 s).[33, 34] The resulting freshly-etched PSi is then chemically oxidized in H_2O:NH_3:H_2O_2 solution in a volumetric ratio of 5:1:1 at 75°C for 1 h to create a hydrophilic $PSiO_2$ matrix. Following oxidation, the $PSiO_2$ samples are chemically modified by silanisation using 2% APTES (diluted in toluene, 1 h), resulting in positively-charged amine groups grafted on to the surface. For bacterial growth experiments, the APTES-modified MPSiAS are further modified with 10 mM SC solution (diluted in acetonitrile, 7 min) and with D-Mannosamine hydrochloride (200 μg mL^{-1}), resulting in mannose-functionalized surface, to promote bacteria adhesion.[35-37]

2.3 Scanning Electron Microscopy

High-resolution scanning electron microscopy (HRSEM) images of the neat MPSiAS are obtained using a FEI Sirion HRSEM instrument at an accelerating voltage (5 keV). Micrographs of the MPSiAS sensors immediately after sensing experiments are obtained using a Carl Zeiss Ultra Plus HRSEM (1 keV). Sensors are fixated using a glutaraldehyde solution (2% in 0.1 M PBS) followed by dehydration through an ethanol series (10% to absolute). Subsequently, the sensors are cross-sectioned using a diamond scriber and sputtered with gold-palladium or carbon.

2.4 Measurement of Interferometric Reflectance Spectra

Interferometric reflectance spectra of the samples are collected using an Ocean Optics charge-coupled device (CCD) USB 4000 spectrometer fitted with a microscope objective lens coupled to a bifurcated fiber-optic cable. A tungsten light source is focused onto the center of the sample surface with a spot size of approximately 1-2 mm^2. Reflectivity data are recorded in the wavelength range of 400-1000 nm, with a spectral acquisition time of 500 ms. Both illumination of the surface and detection of the reflected light are performed along an axis coincident with the surface normal.

2.5 Flow Cell Experiments

MPSiAS samples are placed in a Plexiglas custom-made flow cell in which a buffer solution is first delivered at a rate of approximately 0.1 mL min^{-1}. The reflectivity spectrum is continuously recorded and a baseline is achieved by dosing the buffer for approximately 45 min. The bacteria suspensions are delivered by continuous circulation at a constant flow of 0.1 mL min^{-1} for 45 min. Data points are collected every 15 s.

2.6 Bacteria Culture

E. coli/pGFP is cultivated with 5 mL of Luria-Bertani (LB) broth medium (medium composition in deionized water (1 L): NaCl (5 g), yeast extract (5 g), and tryptone (10 g)). The bacteria are incubated overnight at 37°C with shaking. The bacteria concentration is monitored photometrically by reading the optical density (OD) at a wavelength of 600 nm. After overnight growth in LB medium, the OD_{600} value is measured to determine bacterial concentration. The number of cells is directly proportional to the OD_{600} measurements (1 OD_{600} = 10^8 cells mL^{-1}). Thus, the bacteria concentration is calculated from the OD_{600} measurements. For bacterial growth studies, the bacteria cells are grown to an early exponential phase and diluted to appropriate concentrations for the experiments.

2.7 Bacterial Growth under Confinement Conditions

After the mannose-functionalized MPSiAS were exposed to exponential phase *E. coli* suspensions (10^6 cell mL^{-1}), the samples are scanned using a Carl Zeiss Ultra Plus HRSEM (1 keV). Sensors are prepared for observation as described previously (see section 2.3). Quantification of bacterial capture and growth within the pores is carried out by averaging 100 images (approximately 90 pores in each image) taken at various locations on each MPSiAS surface. Optical monitoring of bacteria growth are carried out using the same setup described in section 2.4. The mannose-functionalized MPSiAS are incubated with *E. coli* suspensions (at a concentration of 10^6 cell mL^{-1}) for 30 min. The sample reflectivity is recorded throughout the experiment.

2.8 Confocal Laser Scanning Microscopy

Immediately after the sensing experiment, the samples are scanned with a LSM 700 confocal laser scanning microscope (Carl Zeiss, Inc) connected to a Zeiss inverted microscope equipped with a Zeiss X63 oil immersion objective. Combinations of 405-nm and 488-nm laser lines are used for the excitation of $PSiO_2$ structure and *E. coli*/pGFP, respectively. For three-dimensional image projection of the porous structure, z-scans in 0.3 μm increments are taken over a depth of ~ 8 microns and projected by using standard Carl Zeiss software (ZEN 2009). Quantification of bacteria entrapped within the pores is carried out by averaging over at least five images taken at various locations on each MPSiAS transducer and used to calculate the 'fill fraction' of the pores.

Cite this: DOI: 10.1039/c0xx00000x

www.rsc.org/xxxxxx

ARTICLE TYPE

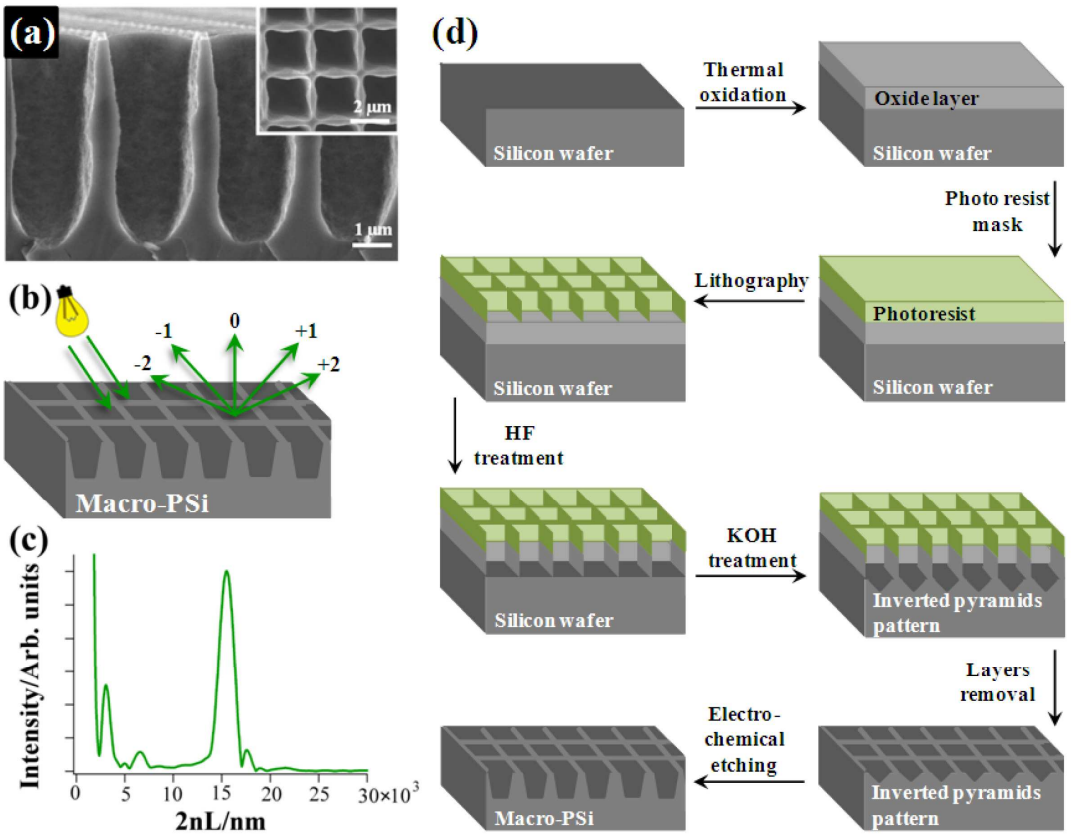

Figure 1. (a) Cross-section view and top view (inset) HRSEM micrographs of a typical MPSiAS. The periodicity is about 2.5 microns while the thickness of the silicon walls is about ~0.5 microns. (b) Schematics of the RIFTS lamellar grating sensor and the diffraction orders. (c) FFT of the resulting reflectivity spectrum of a typical MPSiAS at normal incidence leading to a single peak, whose position and magnitude are monitored upon introduction of an analyte solution. The presence of the bacteria in the pores affects the spectral interference pattern. (d) Preparation scheme of MPSiAS.

3. Results

In the present work, we describe the fabrication and characterization of a new class of two-dimensional (2D) periodic macro-PSi array structure (MPSiAS), where the pore's diameter is designed to fit the size of the target bacteria cells, and demonstrate for the first time its application as an optical sensing platform for the detection of *E. coli* bacteria. Periodic structures of PSi photonic crystals, with pore diameters comparable in size to that of *E. coli* bacteria cells (typical dimensions of 0.8-2 μm),[38] were fabricated by photolithograph followed by electrochemical anodization. The resulting PSi structure (Fig. 1a) acts as a lamellar (or a phase) grating that scatters the reflected light into a set of diffraction orders at various angles according to the relationship between the periodicity of the grating and the optical wavelength (see Fig. 1b). Our recent work describes the detailed optical characteristics of these structures.[39] Briefly, as the reflected light is collected normal to the pore's surface, only the zero-order diffraction is measured (*i.e.*, the backscattered light having θ=0, where θ is the diffraction angle), yielding the following expression for the intensity of the (zero order) reflected light:

$$(1)\quad I(\theta = 0) = I_0 \cos^2\left(\psi_0/2\right)$$

where

$$(2)\quad 2\psi_0 = 2kL = \frac{2\pi}{\lambda}(2n_0 L)$$

I is the intensity of the reflected light, ψ_0 is the phase delay between the incident and the reflected beams, λ is the (free space) optical wavelength, L is the depth of the pores, n_0 is the refractive index of the medium filling the pores, and the term $2n_0L$ is thus

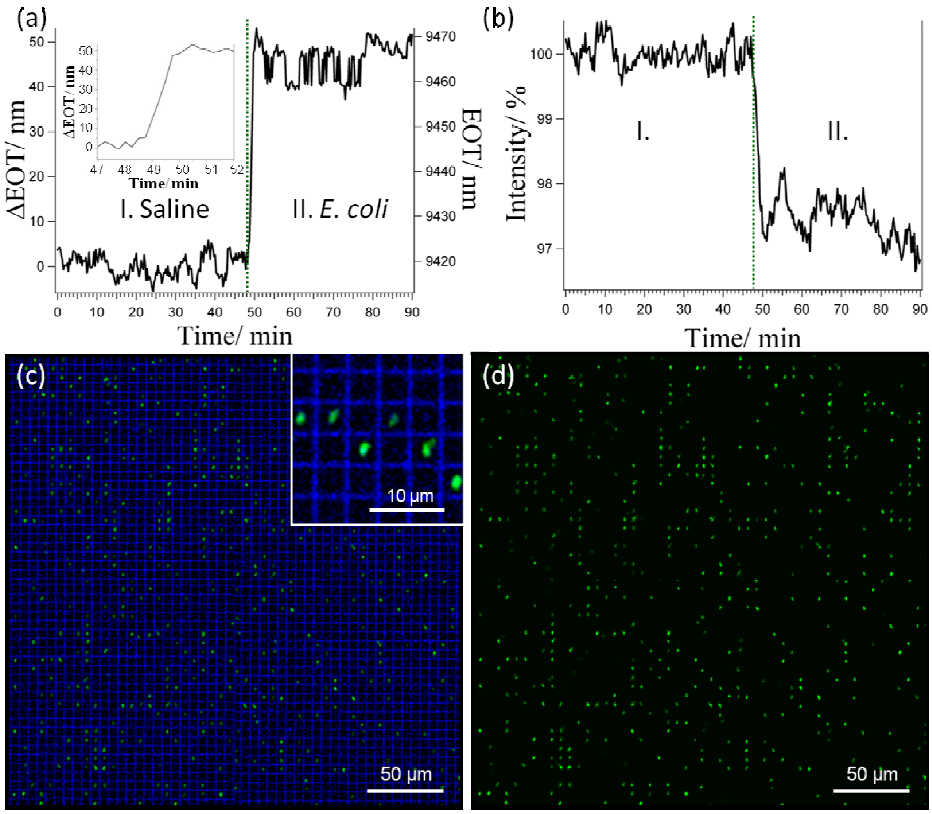

Figure 2. Real time detection of *E. coli* with PSi lamellar gratings. (a) Optical thickness vs. time (in the inset: zoom of the EOT shift); (b) Intensity vs. time; APTES-modified MPSiAS sample is fixed into a flow-cell and the reflectivity spectrum is recorded every 15 s. First, the sample is washed with a saline solution (0.85% w/v NaCl) to acquire a baseline (I) followed by incubation with 10^6 cell mL^{-1} *E. coli* (II); (c-d) CLSM Z-projection images of the sensor immediately after the sensing experiment. (c) Top-down view (x-y plane) inside the porous matrix (8 µm into the z-plane at 63x with oil objective). Green spots: *E. coli*/pGFP bacteria; blue grid: photoluminescence of the oxidized MPSiAS (in the inset: zoom of the captured bacteria inside the pores); (d) Top-down view (x-y plane) inside the porous matrix without the signal from the MPSiAS grid.

the optical path, referred to as the effective optical thickness (EOT) of the lamellar grating. Fast Fourier transform (FFT) of the reflectivity spectrum from the MPSiAS layer provides a direct way to monitor the EOT of the layer, which is characterized by a single peak as shown in Figure 1c (also see Supporting Information Fig. S1, for the raw reflectivity spectrum and corresponding FFT spectrum). Sensing is accomplished once bacteria penetrate into the macro-pores, inducing measurable changes in the EOT that can be monitored and quantified in real-time via RIFTS analysis.

MPSiAS samples, with a periodicity in the range of few microns, are fabricated; the fabrication process is schematically illustrated in Figure 1d. In brief, a 2D pattern of inverted pyramid grooves is defined on top of the Si wafer by alkaline etching via a photolithographic oxide mask. Then, an electrochemical-etching process is performed under dark conditions, using a solution of HF and DMF, at a constant current density. Figure 1a presents cross-section and top view (inset) HRSEM images of a typical MPSiAS, showing 2D ordered array of cylindrical pores having rectangular cross-section profile. Two groups of structures, with a periodicity of 2.5 µm and 4 µm, and a typical depth of 4 µm, were fabricated to allow a facile entrapment of the bacteria cells within the array. Following anodisation, the resulting freshly etched PSi is chemically oxidized to create a hydrophilic porous SiO_2 matrix ($PSiO_2$). Next, the oxidized MPSiAS samples are modified with 3-aminopropyltriethoxy silane (APTES) in order to functionalize the porous surface with positively charged amine groups. As most bacteria carry a net negative surface charge, adhesion of *E. coli* is promoted on positively charged surfaces.[40]

Preliminary sensing experiments are carried out by exposure of the APTES-modified MPSiAS to *E. coli* bacteria suspensions. The sensors are fixed in a custom-made flow cell in order to assure that the samples reflectivity is recorded at the same spot during the entire measurement. Bacteria suspensions (10^5 to 10^7 cell mL^{-1} in saline) are continuously delivered and the reflectivity spectra of the sensors are collected using a CCD spectrometer and analysed by applying FFT. Figure 2 summarizes the results of a typical sensing experiment. In this figure the changes in the FFT spectrum before and after the introduction of *E. coli* bacteria (10^6 cell mL^{-1}) are depicted as function of time. Sensing is accomplished by measuring the variation in the EOT and the

Cite this: DOI: 10.1039/c0xx00000x

www.rsc.org/xxxxxx

ARTICLE TYPE

Table 1. Results of sensing experiments for different MPSiAS and comparison between the 'fill fraction' values predicted by the model and the corresponding 'fill fraction' obtained from the confocal microscopy images.

Sample no.	Periodicity of pores [μm]	Pores depth [μm]	ΔEOT [nm]	ΔEOT/EOT	Fill fraction by model [%]	Fill fraction by CLSM [%]
1	4	3.5	45±5	0.0048	25±7	21±1
2	4	4	38±10	0.0036	8±4	7±3
3	2.5	2.5	8±2	0.0013	2±1	1.6±0.4
4	2.5	7.5	4±2	0.0002	4±2	3±1

intensity of the sensor once the bacteria cells are trapped inside the pores. Upon bacteria introduction a rapid increase in EOT of approximately 45 nm is observed (Fig. 2a). This EOT change is attributed to the entrapment of bacteria into the pores, leading to a refractive index increase. Simultaneously, a decrease in the reflectance intensity (of about 3%) can be observed (Fig. 2b) most probably due to light scattering induced by the bacteria cells.[19, 21, 22]

To validate the results of the RIFTS, the sensors are carefully studied by a confocal laser-scanning microscope (CLSM) immediately after the sensing experiment. Confocal microscopy is used as a complementary tool for confirming and quantifying the amount of captured bacteria within the 2D array of pores. In addition, CLSM allows determining whether the captured cells are floating on top the sensor's surface (but not inside the pores) or entrapped within the pores. Green fluorescent protein-expressing *E. coli* (*E. coli*/pGFP) (excitation wavelength, λ_{ex}=488 nm) and photoluminescence (PL) of the $PSiO_2$ (λ_{ex}=405 nm) are detected in z direction from the upper surface into the pores over a depth of ~8 microns with a scanning step of 0.3 μm. A CLSM movie of a sensor immediately after sensing experiment (see Figure S2, Supporting Information (movie)) illustrates the ability of the CLSM technique to distinguish between bacteria that are floating above the porous structure to cells that are entrapped in the pores. As the blue signal from the porous array is observed (assigned to the PL from oxidized PSi), the focal plane is approximately at the same level of the upper oxidized PSi surface.[41] The data confirm that the bacteria cells have infiltrated into the porous layer and are entrapped within the pores. Figure 2c depicts top-down view (x-y plane) CLSM images of MPSiAS immediately after the sensing experiment, in which *E. coli*/pGFP bacteria are introduced at a concentration of 10^6 cell mL^{-1}. The bacteria are clearly observed to be captured inside the pores. By subtracting the PL signal of the top oxidized PSi from that of the MPSiAS sensor, an ordered pattern of the trapped bacteria is observed; revealing the large number of cells that are imprisoned within the pores, see Figure 2d. Careful analysis of this figure shows differences in the fluorescence signal intensity from the captured GFP-expressing bacteria, indicating that the cells are positioned in different depths inside the pores. From image analysis of the CLSM data we can quantify the relative number of pores occupied by bacteria, this value will be referred as the 'fill fraction' of the MPSiAS. The 'fill fraction' values for MPSiAS sensors, characterized by different periodicities of 2.5 and 4 μm, are summarized in Table 1. These values are calculated by averaging at least 5 CLSM images taken at different locations for each sensor.

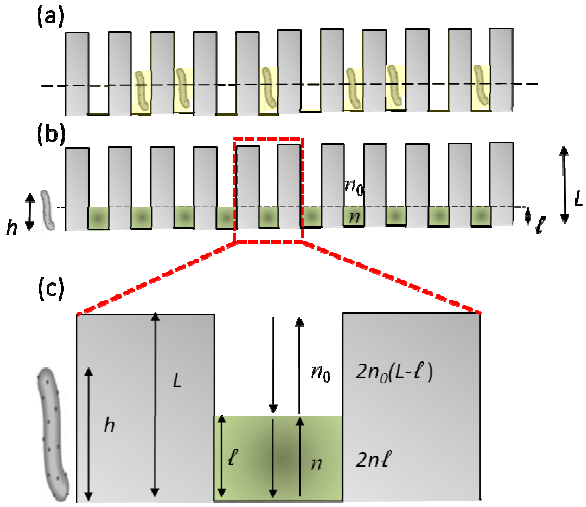

Figure 3. A schematic illustration of the model developed for correlating the optical readout and the bacteria 'fill fraction'. (a) Schematics of the RIFTS lamellar grating sensor with bacteria trapped in the pores. (b) The bacteria trapped in the pores are replaced by a continuous effective layer having a thickness (ℓ) and a refractive index (n). (c) Schematics of the mathematical model, which used to simulate sensing experiments.

Next, a simple model aimed at simulating the results of the

Cite this: DOI: 10.1039/c0xx00000x

www.rsc.org/xxxxxx

ARTICLE TYPE

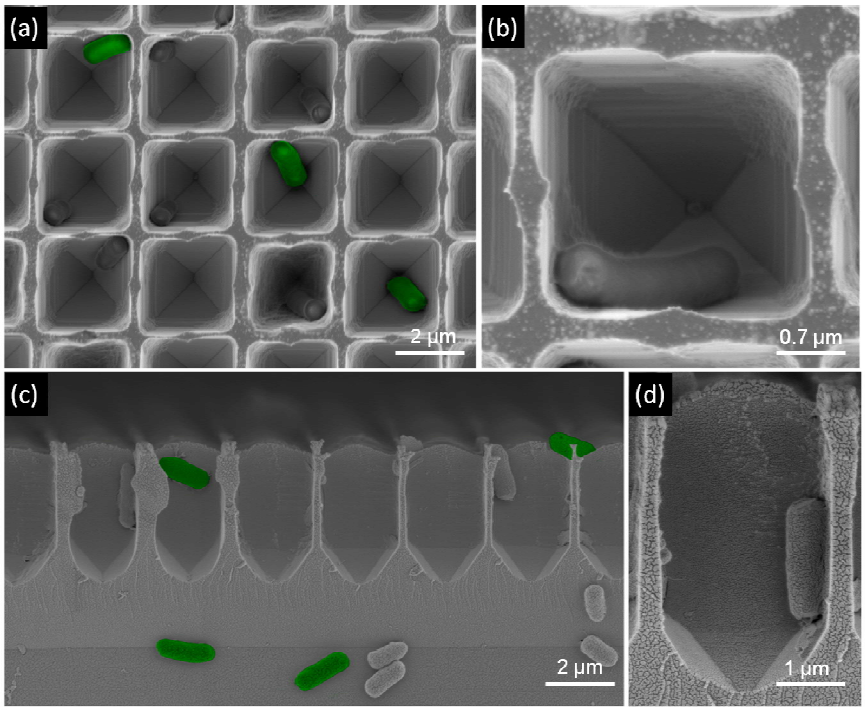

Figure 4. HRSEM images of MPSiAS following the sensing experiment, demonstrating bacteria cells confined within the pores. Some of the bacteria cells are false-colored to ease observation. (a-b) Top–view micrographs of the sensor and (c-d) Cross-sectional micrographs of the sensor. Note that bacteria observed to adhere to the bulk Si (below the porous layer) in image (c) have probably detached from their pore location during sample fracturing and processing for observation.

sensing experiments, is adapted in order to correlate between the optical readout of the sensor i.e., EOT shift, and the bacteria concentration (i.e., the 'fill fraction' as measured by the CLSM technique).[39] Figure 3 schematically illustrates the concept of the model, where pores containing trapped bacteria are replaced by an effective layer of thickness, ℓ, and refractive index, n. Thus, for a given EOT shift, the model predicts the corresponding 'fill fraction'. The refractive indices of the bacteria and the host saline solution are taken to be 1.4 (n) and 1.33 (n_0) respectively,[42, 43] so that the only free parameter in the model is the effective thickness of the filled pores, or equivalently the 'effective fill factor' (*eff*) defined as (in two-dimensions), $eff = (\ell/L)^2$ where, L is the pore depth. This quantity can be estimated from the model presented in Figure 3(c) to be:

$$(3)\quad eff = \frac{\Delta EOT / EOT}{\Delta n / n_0}$$

where $\Delta(EOT)/EOT$ is the relative change of the EOT as measured during the sensing experiment and, $\Delta n = n - n_0$, is the absolute change of the refractive index due to bacteria capture. The fill fraction of the MPSiAS can directly be related to the 'effective fill factor' as follows:

$$(4)\ fill\ fraction = eff \cdot \left(\frac{\text{volume}_{\text{pores}}}{\text{volume}_{\text{E.coli}}} \right)$$

Table 1 presents measured ΔEOT values for different sensing experiments and the corresponding 'fill fraction', calculated by the model. MPSiAS with high periodicity i.e., larger pores, exhibit greater EOT shifts, corresponding to superior bacteria capture. The model results are in fairly good agreement with the 'fill fraction' estimated from the CLSM images indicating that, despite of the model's approximations, it provides a reasonable description to the sensing events. For example, for sample 1 (Table 1), the model predicts a 'fill fraction' of ~25%, while the CLSM data yields a 'fill fraction' value of approximately 21%.

The MPSiAS sensors are exposed to different *E. coli* suspensions, in the range of 10^5-10^7 cells mL^{-1}, in order to study the correlation between the obtained optical signal and the bacteria concentration. For pores with a periodicity of 2.5 µm the optical response is proportional to the bacteria suspension concentration; higher bacteria concentration results in larger EOT changes (see Table S1, Supporting Information). Upon exposure to 10^5 cells mL^{-1} suspension no change in the EOT value is observed. For sensors with pores periodicity of 4 µm, higher ΔEOT values are obtained for similar bacteria concentrations, due to the larger pore

Cite this: DOI: 10.1039/c0xx00000x

www.rsc.org/xxxxxx

ARTICLE TYPE

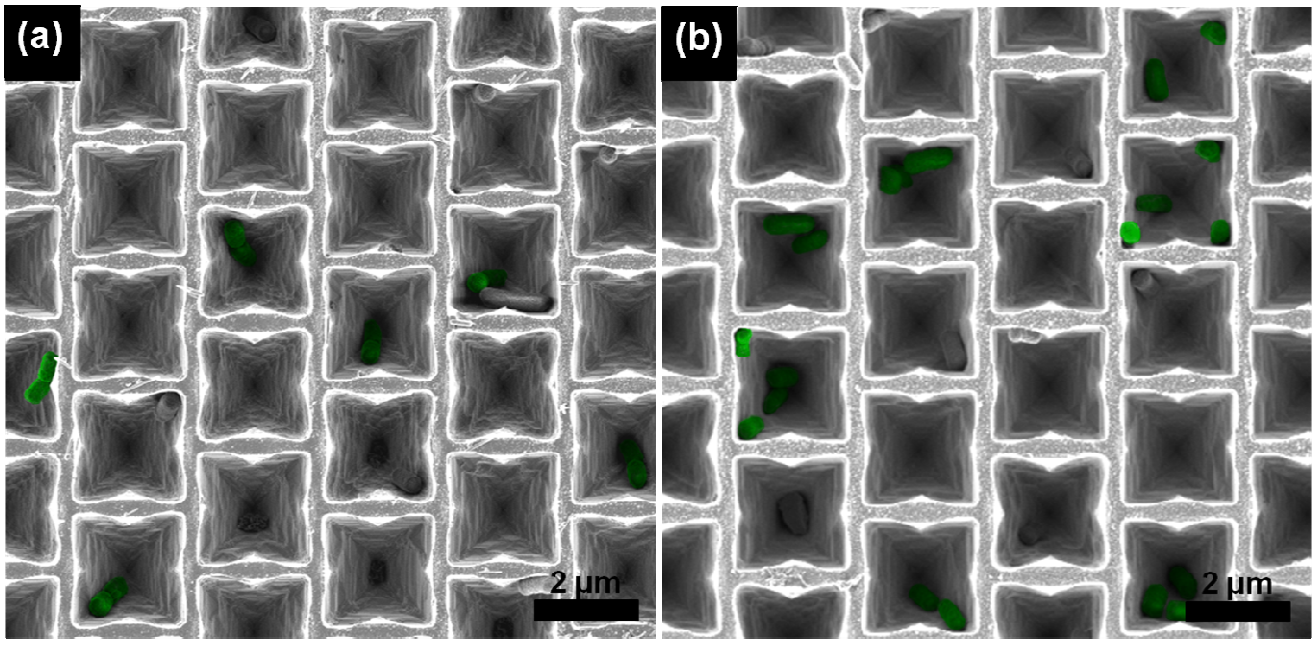

Figure 5. Top-view HRSEM images of MPSiAS sensors following bacterial growth experiment. (a) Control sensor (no incubation); bacteria undergoing cell division are false-colored. These cells display elongated morphology and formation of a septum. (b) An incubated sensor, in which individual pores are populated with several bacteria cells. Some of the bacteria cells are false-colored to ease observation.

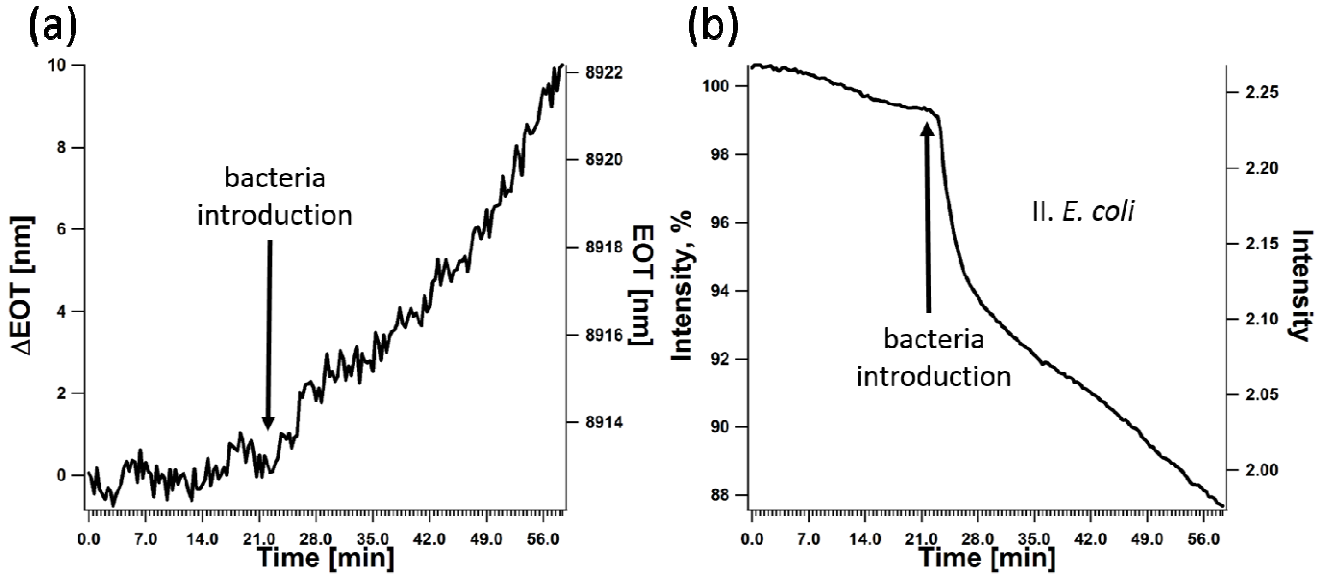

Figure 6. Real time monitoring of *E. coli* growth. (a) Optical thickness vs. time; (b) Intensity vs. time; mannose-functionalized MPSiAS sensors is fixed in a cell and the reflectivity spectrum is recorded every 20 s. Arrow indicates the introduction of *E. coli* suspension (10^6 cell mL^{-1} in LB at 37ºC).

Cite this: DOI: 10.1039/c0xx00000x

www.rsc.org/xxxxxx

ARTICLE TYPE

dimensions. Moreover, in this case, exposure to 10^5 cells mL^{-1} suspension induces a change of 3 nm in EOT.

In order to study how the *E. coli* cells are attached to the porous array surface and their arrangement within the individual pores, the MPSiAS samples are investigated by SEM immediately after the sensing experiments. Top-view and cross-sectional high-resolution SEM images of MPSiAS sensors are presented in Figure 4, revealing that most of the bacteria cells are localized within the pores of the array. While, only few cells appear to be adhered to the upper surface, see Figure 4c. Careful study of the top-view micrographs (Fig. 4a,b) indicates the preference of the cells to assemble and adhere to the corners of the rectangular pores, suggesting that the bacteria tend to maximize their contact area with the surface.

In order to show the potential applicability of these structures as a platform for monitoring of bacteria viability, we have further functionalized the APTES-modified MPSiAS with SC cross-linker and with D-mannosamine hydrochloride. It is well established that pathogens bind to carbohydrates displayed by the cells that they infect.[44, 45] For example, *E. coli* bind to mannose via bacterial-surface lectins expressed on the bacterium cell surface.[46] Bacterial growth under confinement conditions may allow for subsequent monitoring the growth of individual bacteria at the single cell level after their entrapment. Thus, the mannose-functionalized MPSiAS is exposed to exponential phase *E. coli* suspensions (10^7 cell mL^{-1}); the incubation time is set to 1 h, to assure bacteria infiltration and capture within the pores. Subsequently, the samples are washed using LB medium, to remove unbound bacteria. At this time point, some of the samples are fixated and are used as a control. While, the other MPSiAS sensors are further incubated at 37ºC, to allow bacterial growth within the pores. Following incubation, the samples are also fixated and studied by HRSEM, see Figure 5.

Preliminary experiments for optical monitoring bacterial viability and growth are carried out by incubating the mannose-functionalized MPSiAS with early exponential phase *E. coli* bacteria suspensions (10^6 cell mL^{-1} in LB at 37ºC). The reflectivity spectrum is collected during the course of the experiment. Figure 6 summarizes the results of a typical bacterial growth experiment. Upon bacteria introduction a rapid increase in EOT of approximately 3 nm is observed (Fig. 6a). This EOT change is attributed to the entrapment of bacteria into the pores. Then, a steady exponential increase of the EOT is observed, which is assigned to bacterial growth within the pores. Simultaneously, a rapid decrease in the reflectance intensity (of about 5-6%) can be observed (Fig. 6b) immediately when the bacteria are introduced followed by a continuous exponential decrease in the intensity.

3. Discussion

This work presents a new concept for the design of optical sensors that can detect in real-time cell capture events. The sensor is based on a 2D periodic structure of PSi photonic crystals in which the pore's size is tuned to fit the size of the target *E. coli* bacteria cells. The zero-order diffraction of the light reflected from these PSi arrays presents a spectral interference pattern according to the phase accumulated inside the pores, as illustrated in Figure 1b. Spontaneous bacteria capture within the pores is achieved by proper design of the MPSiAS periodicity and its surface chemistry. Aizenberg et al.[42, 43, 47-49] recently reported on similar phenomena of spontaneous bacteria patterning and oriented attachment on arrays of high-aspect-ratio (HAR) nano- and micro- structures. It should be noted that in these studies the bacteria were cultured on the HAR surfaces and monitored for 4-48 h. Tuning the periodicity of the HAR arrays within the relevant cellular bacteria scale resulted in distinctive differences in bacterial assembly, allowing for direct cell patterning over large areas (at the microscopic scale).

Herein, we show that a spontaneous bacteria patterning (Fig. 2c,d) occurs upon exposure of the MPSiAS to *E. coli* suspensions at different concentrations. Continuous monitoring of the optical interference spectra of these MPSiAS during bacteria introduction, results in a rapid increase in EOT (Fig. 2a), attributed to the entrapment of bacteria cells within the porous array. Simultaneously, a decrease in the reflectance intensity is detected, ascribed to light scattering by the captured cells (Fig. 2b). Thus, in a close analogy to conventional RIFTS sensors,[4, 5] changes in the reflected light are correlated to cells localization within the pores, allowing for real-time detection of bacteria.

Our preliminary optical studies demonstrate a detection limit of 10^4 cell mL^{-1} for *E. coli*. It should be emphasized that no bioreceptors e.g., antibodies, are used in this case to capture the bacteria. Thus, the present sensor scheme can be potentially applicable for evaluation of total bacteria count, providing information on the existence of bacteria in a sample. Such techniques that quantify the total number of bacteria, regardless of their type, are important in the food and water industries, and are employed in many cases as an indicator of the quality and suitability for human consumption.[50] Whereas, for selective bacteria detection, appropriate capture probes, such as antibodies[21, 22] or aptamers,[51-53] should be immobilized onto the MPSiAS pore walls. We have already demonstrated that immobilization of appropriate monoclonal antibodies onto mesoporous Si transducers via versatile conjugations routes[19-22, 25] allows for specific detection of *E. coli* bacteria. Thus, the similar

approaches can be used for incorporation of recognition elements to the MPSiAS sensors.

A simple model that correlates the optical readout of the sensor and the bacteria concentration is developed. Thus, for a given EOT shift, the model predicts the corresponding value of the 'fill fraction'. Confocal microscopy is used as a complementary tool to estimate the concentration of trapped bacteria and to validate the model results. The model predictions are found to be in good agreement with the confocal microscopy data, see Table 1. The deviations between the 'fill fraction' values are mainly attributed to the model assumptions. First, the model refers to the bacteria as a homogenous liquid filling the pores. This assumption oversimplifies the complex structure of the cell and its heterogeneity. Second, as the reflected light is collected normal to the pore's surface, only the intensity of the zero-order diffraction is measured. Therefore, due to pore morphology of the MPSiAS (see Fig. 1a) the model takes into consideration a diameter of about 25% of the opening of the pore for the effective coherent reflective surface, which is used to calculate the effective pore volume and hence the resulting fill fraction. Another cause for deviation may result from the difference in spot size of the optical data that is collected in the experimental sensing setup and the CLSM. In our sensing setup, the EOT signal is measured from a single spot (with a typical diameter of 1 mm), while CLSM measurements are averaged over five different areas of the sensor's surface.

By using HRSEM, we study how *E. coli* cells are attached and arranged within the porous array. The HRSEM micrographs indicate that the bacteria cells tend to maximize their contact area with the pores and prefer to attach and localize in the pores' corner regions (Fig. 4). The potential applicability of mannose-functionalized MPSiAS structures as a platform for detection of bacteria viability or monitoring bacterial growth behaviour/rate is studied by incubating the sensors (post bacteria capture step) under optimal conditions (LB medium, 37°C). HRSEM studies of these sensors in comparison to control sensors (no incubation) were carried out in order to investigate *E. coli* bacterial growth within the porous array (Fig. 5). These studies reveal that most of the captured bacteria (control, no incubation) appear to be at the septal constriction stage of division cell cycle (Fig. 5a). *E. coli* bacteria, undergoing binary fission, exhibit at this stage elongated morphology (to twice of their original length) and formation of a septum at mid-cell.[54, 55] As the sensors are exposed to bacteria suspensions, in which cells were grown to an early exponential phase, this behaviour is expected. In the incubated MPSiAS sensors (Fig. 5b), most cells are individual, ascribed to septum completion and separation to two daughter cells. These results suggest that the bacteria are able to proliferate and grow when confined in these porous structures. Assessment of bacterial capture and growth within the pores is carried out by averaging 100 images (approximately 90 pores in each image) taken at various locations on each MPSiAS. The samples are carefully investigated to quantify the following numbers: pores occupied by a single bacterium, pores occupied by two bacterial cells, pores occupied by three or more cells. Results reveal that in the incubated sensors, the populated pores contain several bacteria cells (≥2), whereas, in the control sensors most of the pores are occupied by a single cell. The number of pores populated by two cells and by three or more cells, is two- and three-fold higher (respectively) in comparison to the control sensors (no incubation). Thus, these results demonstrate that under proper conditions, the confined *E. coli* bacteria cells can proliferate and grow within the individual pores. Furthermore, preliminary experiments demonstrate the possibility to optically monitor the growth of the confined bacteria in a continuous manner. The results show a continuous increase in the EOT of the sensor during bacteria growth, in agreement with higher number of bacteria cells observed by HRSEM studies. This approach could be potentially adapted for improving current live/dead bacterial assays.

Conclusions

We show that monitoring changes in the optical interference spectra of the MPSiAS sensors enables a simple and sensitive detection of the bacteria. This proof of concept work extends the current sensing capabilities of PSi optical transducers and provides a generic label-free sensing platform that is applicable for rapid detection and identification of a variety of microorganisms e.g., bacteria, fungi and viruses. Future work will explore the use of specific recognition elements e.g., antibodies and aptamers with high affinity to the target bacteria, in order to increase the sensor sensitivity and selectivity.

Author Contributions

Y.M, A.N and E.E fabricated and characterized the MPSiAS sensors, and built the model for correlating the optical readout. N.M-I characterized the optical properties of MPSiAS sensors, carried out the bacteria sensing experiments and confocal microscopy studies together with L.M.B. N.B.D has carried out bacteria growth and viability studies. All authors discussed the results and implications at all stages. E.S and A.S have conceived the research, designed the study, and analysed data. N.M-I and E.S wrote the manuscript with input from all authors.

Acknowledgments

This work was supported by the ISRAEL SCIENCE FOUNDATION (grant No. 1146/12) and by the Israeli Ministry of Science (grant no. 3-6798). E.S thanks the Marie Curie Reintegration Grant administered by the European Union, the Russell Berrie Nanotechnology Institute (RBNI) and the Lorry I. Lokey Center for Life Science and Engineering. N.M-I is most grateful for the Promotion of Women in Sciences and Engineering Fellowship by the Israeli Ministry of Science and for the Russell Berrie Scholarships for Outstanding Graduate Students by the Russell Berrie Nanotechnology Institute. L.M.B acknowledges the Lady Davis Trust for a postdoctoral fellowship. The authors thank Ms. Elena Tenenbaum and Mrs. Adi Balter for their help in obtaining high-resolution SEM images of the MPSiAS sensors.

Notes and references

[a] *Department of Biotechnology and Food Engineering, Technion – Israel Institute of Technology, Haifa 32000, Israel. Fax: 972 4829 3399; Tel: 972 4829 5071; E-mail: esegal@tx.technion.ac.il*

[b] *Racah Institute of Physics and the Harvey M. Krueger Family Center for Nanoscience and Nanotechnology, The Hebrew University of Jerusalem, Jerusalem 91904, Israel.*

[c] *The Russell Berrie Nanotechnology Institute, Technion – Israel Institute of Technology, Haifa 32000, Israel.*

**Correspondence should be addressed to E.S. (esegal@tx.technion.ac.il)*

†Electronic Supplementary Information (ESI) available: Figure S1: (a) A reflectivity spectrum of a typical MPSiAS sensor. (b) FFT of the reflectivity spectrum is performed, leading to a single peak, whose position and magnitude are monitored upon introduction of an analyte solution. Figure S2: A CLSM movie of a sensor immediately after sensing experiment illustrates the ability of the CLSM technique to distinguish between bacteria that are floating above the porous structure to cells that are entrapped in the pores. Table S1. Optical response of MPSiAS sensors, having 2.5 and 4 μm pore periodicity, upon introduction of different concentrations of *E. coli* suspensions. See DOI: 10.1039/b000000x/

References

1. L. M. Bonanno and E. Segal, *Nanomedicine*, 2011, **6**, 1755-1770.
2. A. Jane, R. Dronov, A. Hodges and N. H. Voelcker, *Trends Biotechnol*, 2009, **27**, 230-239.
3. M. M. Orosco, C. Pacholski, G. M. Miskelly and M. J. Sailor, *Advanced Materials*, 2006, **18**, 1393-1396.
4. C. Pacholski, M. Sartor, M. J. Sailor, F. Cunin and G. M. Miskelly, *J. Am. Chem. Soc.*, 2005, **127**, 11636-11645.
5. C. Pacholski, C. Yu, G. M. Miskelly, D. Godin and M. J. Sailor, *J. Am. Chem. Soc.*, 2006, **128**, 4250-4252.
6. M. J. Sailor and J. R. Link, *Chemical Communications*, 2005, 1375-1383.
7. M. P. Schwartz, S. D. Alvarez and M. J. Sailor, *Analytical Chemistry*, 2007, **79**, 327-334.
8. M. P. Schwartz, A. M. Derfus, S. D. Alvarez, S. N. Bhatia and M. J. Sailor, *Langmuir*, 2006, **22**, 7084-7090.
9. C. K. Tsang, T. L. Kelly, M. J. Sailor and Y. Y. Li, *ACS Nano*, 2012, **6**, 10546-10554.
10. S. M. Weiss, G. Rong and J. L. Lawrie, *Physica E: Low-dimensional Systems and Nanostructures*, 2009, **41**, 1071-1075.
11. B. Sciacca, F. Frascella, A. Venturello, P. Rivolo, E. Descrovi, F. Giorgis and F. Geobaldo, *Sensors and Actuators B-Chemical*, 2009, **137**, 467-470.
12. L. M. Bonanno, T. C. Kwong and L. A. DeLouise, *Analytical Chemistry*, 2010, **82**, 9711-9718.
13. G. Rong, J. D. Ryckman, R. L. Mernaugh and S. M. Weiss, *Appl. Phys. Lett.*, 2008, **93**, 161109-161103.
14. D. Zhang and E. C. Alocilja, *Ieee Sensors Journal*, 2008, **8**, 775-780.
15. K. P. S. Dancil, D. P. Greiner and M. J. Sailor, *J. Am. Chem. Soc.*, 1999, **121**, 7925-7930.
16. V. S. Y. Lin, K. Motesharei, K. P. S. Dancil, M. J. Sailor and M. R. Ghadiri, *Science*, 1997, **278**, 840-843.
17. B. L. Miller, in *Optical Guided-wave Chemical and Biosensors II*, eds. G. Urban, M. Zourob and A. Lakhtakia, Springer, 2010, pp. 3-26.
18. S. D. Alvarez, M. P. Schwartz, B. Migliori, C. U. Rang, L. Chao and M. J. Sailor, *Physica Status Solidi a-Applications and Materials Science*, 2007, **204**, 1439-1443.
19. N. Massad-Ivanir, G. Shtenberg and E. Segal, *In Nano Bio-Technology for Biomedical and Diagnostics Research*, 2012, **733**, 37-45.
20. N. Massad-Ivanir, G. Shtenberg and E. Segal, *The Journal of Visualized Experiments*, 2013, **81**, e50805.
21. N. Massad-Ivanir, G. Shtenberg, A. Tzur, M. A. Krepker and E. Segal, *Analytical Chemistry*, 2011, **83**, 3282-3289.
22. N. Massad-Ivanir, G. Shtenberg, T. Zeidman and E. Segal, *Advanced Functional Materials*, 2010, **20**, 2269-2277.
23. M. P. Doyle, L. R. Beuchat and T. J. Montville, eds., *Food Microbiology: Fundamentals and Frontiers* 2 Sub edition edn., ASM Press Washington, 2001.
24. C. Kaittanis, S. Santra and J. M. Perez, *Advanced Drug Delivery Reviews*, 2010, **62**, 408-423.
25. N. Massad-Ivanir and E. Segal, in *Porous silicon for biomedical applications*, ed. H. A. Santos, Woodhead Publishing Limited, Cambridge, 2014.
26. G. Recio-Sanchez, G. Dominguez-Canizares, M. Manso, I. Preda, V. Torres-Costa, A. Gutierrez, L. Soriano and R. J. Martin-Palma, *Current Nanoscience*, 2011, **7**, 178-182.
27. L. Su, W. Jia, C. Hou and Y. Lei, *Biosensors and Bioelectronics*, 2011, **26**, 1788-1799.
28. V. Velusamy, K. Arshak, O. Korostynska, K. Oliwa and C. Adley, *Biotechnology Advances*, 2010, **28**, 232-254.
29. D. Ivnitski, I. Abdel-Hamid, P. Atanasov and E. Wilkins, *Biosens. Bioelectron.*, 1999, **14**, 599-624.
30. *CDC - Get Smart: Antibiotic Resistance Questions and Answers, http://www.cdc.gov/getsmart/antibiotic-use/antibiotic-resistance-faqs.html, 2010.*
31. P. Kinnunen, B. H. McNaughton, T. Albertson, I. Sinn, S. Mofakham, R. Elbez, D. W. Newton, A. Hunt and R. Kopelman, *Small*, 2012, **8**, 2477-2482.
32. P. Leonard, S. Hearty, J. Brennan, L. Dunne, J. Quinn, T. Chakraborty and R. O'Kennedy, *Enzyme and Microbial Technology*, 2003, **32**, 3-13.

33. N. Gutman, A. Armon, A. Osherov, Y. Golan and A. Sa'ar, *Physica Status Solidi a-Applications and Materials Science*, 2009, **206**, 1290-1294.
34. N. Gutman, A. Armon, A. Sa'ar, A. Osherov and Y. Golan, *Appl. Phys. Lett.*, 2008, **93**, 3.
35. K. A. Krogfelt, H. Bergmans and P. Klemm, *Infect. Immun.*, 1990, **58**, 1995-1998.
36. I. Ofek, D. Mirelman and N. Sharon, *Nature*, 1977, **265**, 623-625.
37. G. E. Soto and S. J. Hultgren, *J. Bacteriol.*, 1999, **181**, 1059-1071.
38. S. Sundararaj, A. Guo, B. Habibi-Nazhad, M. Rouani, P. Stothard, M. Ellison and D. S. Wishart, *Nucleic Acids Research*, 2004, **32**, D293-D295.
39. Y. Mirsky, A. Nahor, E. Edrei, N. Massad-Ivanir, L. M. Bonanno, E. Segal and A. Sa'ar, *Appl. Phys. Lett.*, 2013, **103**.
40. B. Gottenbos, D. W. Grijpma, H. C. van der Mei, J. Feijen and H. J. Busscher, *Journal of Antimicrobial Chemotherapy*, 2001, **48**, 7-13.
41. S. Inoue, in *Handbook of biological confocal microscopy, Second edition*, 1995, pp. 1-17.
42. A. I. Hochbaum and J. Aizenberg, *Nano Letters*, 2010, **10**, 3717-3721.
43. P. Kim, W. E. Adorno-Martinez, M. Khan and J. Aizenberg, *Nature Protocols*, 2012, **7**, 311-327.
44. M. D. Disney, J. Zheng, T. M. Swager and P. H. Seeberger, *J. Am. Chem. Soc.*, 2004, **126**, 13343-13346.
45. D. L. Jack, N. J. Klein and M. W. Turner, *Immunol. Rev.*, 2001, **180**, 86-99.
46. Z. Barshavit, R. Goldman, I. Ofek, N. Sharon and D. Mirelman, *Infect. Immun.*, 1980, **29**, 417-424.
47. A. K. Epstein, A. I. Hochbaum, P. Kim and J. Aizenberg, *Nanotechnology*, 2011, **22**, 8.
48. R. S. Friedlander, H. Vlamakis, P. Kim, M. Khan, R. Kolter and J. Aizenberg, *Proceedings of the National Academy of Sciences of the United States of America*, 2013, **110**, 5624-5629.
49. P. Kim, A. K. Epstein, M. Khan, L. D. Zarzar, D. J. Lipomi, G. M. Whitesides and J. Aizenberg, *Nano Letters*, 2012, **12**, 527-533.
50. A. Bajwa, S. T. Tan, R. Mehta and B. Bahreyni, *Sensors*, 2013, **13**, 8188-8198.
51. X. X. Cao, S. H. Li, L. C. Chen, H. M. Ding, H. Xu, Y. P. Huang, J. Li, N. L. Liu, W. H. Cao, Y. J. Zhu, B. F. Shen and N. S. Shao, *Nucleic Acids Research*, 2009, **37**, 4621-4628.
52. N. Paniel, J. Baudart, A. Hayat and L. Barthelmebs, *Methods*, 2013, **64**, 229-240.
53. H. M. So, D. W. Park, E. K. Jeon, Y. H. Kim, B. S. Kim, C. K. Lee, S. Y. Choi, S. C. Kim, H. Chang and J. O. Lee, *Small*, 2008, **4**, 197-201.
54. M. T. Madigan, J. M. Martinko and J. Parker, *Brock Biology of Microorganisms*, Tenth edn., Pearson Education, Inc., USA, 2003.
55. M. Vicente, A. I. Rico, R. Martinez-Arteaga and J. Mingorance, *J. Bacteriol.*, 2006, **188**, 19-27.

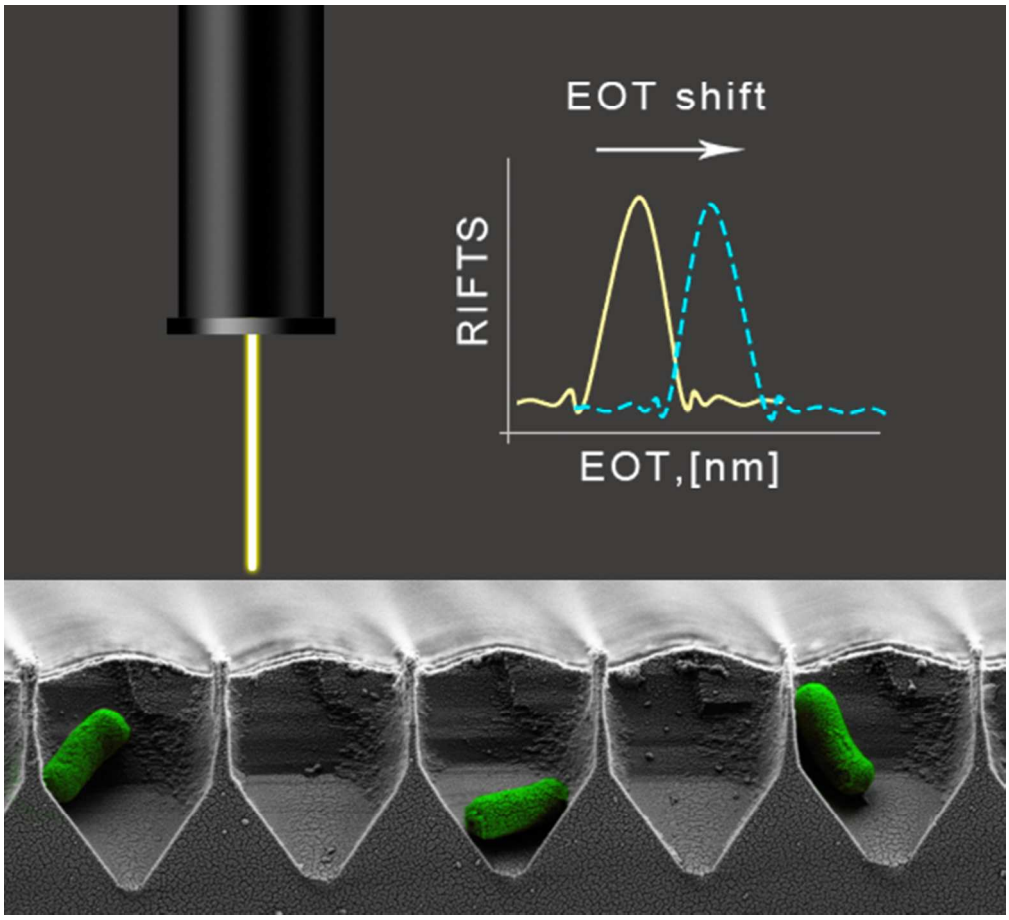

This work introduces a new concept for the design of self-reporting optical structures that can detect and quantify bacteria in real-time. The sensor is based on a two-dimensional periodic structure of porous Si photonic crystals in which the pore size is adjusted to fit the target bacteria cells (Escherichia coli). we demonstrate that sensing scheme can be easily modified to potentially allow monitoring of concentration, growth and physiological state of bacteria cells.
55x50mm (300 x 300 DPI)